A non-rigid registration method for mouse whole body skeleton registration

Di Xiao*[a], David Zahra[b], Pierrick Bourgeat[a], Paula Berghofer[b], Oscar Acosta Tamayo[a], Catriona Wimberley[b], Marie Claude Gregoire[b], Olivier Salvado[a]

[a]The Australian e-Health Research Center, ICT, CSIRO, Australia
[b]Radiopharmaceutical Research Institute, ANSTO, Australia

ABSTRACT

Micro-CT/PET imaging scanner provides a powerful tool to study tumor in small rodents in response to therapy. Accurate image registration is a necessary step to quantify the characteristics of images acquired in longitudinal studies. Small animal registration is challenging because of the very deformable body of the animal often resulting in different postures despite physical restraints. In this paper, we propose a non-rigid registration approach for the automatic registration of mouse whole body skeletons, which is based on our improved 3D shape context non-rigid registration method. The whole body skeleton registration approach has been tested on 21 pairs of mouse CT images with variations of individuals and time-instances. The experimental results demonstrated the stability and accuracy of the proposed method for automatic mouse whole body skeleton registration.

Keywords: 3D non-rigid registration, mouse whole body skeleton registration, 3D shape context model

1. INTRODUCTION

Small animal imaging is increasingly used as a pre-clinical tool to identify new imaging agent, or assess effectiveness of therapy of diseases through their MRI, micro-CT and Position Emission Tomography (PET) images *in vivo*. This involves scanning a cohort of small rodents (typically mice and rats), and computing population statistics of specific organs or measuring and quantifying temporal changes in a region of interest (ROI).

One challenging step to study a large numbers of individual animals is performing spatial normalization before any subsequent processing. Common tasks include the tracking of tumor size variations and shape in a longitudinal experiment of rats or mice CT/PET images acquired over time or mapping specific organs from an atlas to any new scanned images. For small animals, because of the articulated joints and their anatomical structures, it is challenging to position the animals in a same position with a same posture for each scan. The use of physical support for the animals reduces large posture differences but a significant deformation of the animal body still exists from one scan to another and between different animals. The only easily identifiable and robust anatomical features present in CT images are the skeletons, lungs and skin.

Recently, a few methods have been proposed to address the automatic registration of small animal whole body skeletons. Baiker *et al.* proposed an automatic articulated registration method for mouse skeleton registration by identifying joints and individual bones and traversing a hierarchical mouse skeleton tree predefined and registering each part by iterative closest point (ICP) from a coarse to fine method [1]. Li *et al.* [2] proposed using robust point-based registration [3] and softassign algorithm [4] for mouse whole body skeleton registration in their two-step registration process and tested it on a mouse's serial CT images. Hesheng *et al.* [5] proposed a deformable image registration method, consisting of a global affine transformation and a local B-splines deformation, for mouse whole body skeleton registration. The deformation model was incorporated into robust point matching (TPS-RPM) [3] method for estimating point correspondences and surface deformation. The first method is a combination of piecewise rigid registration methods for automatically labeling of whole body skeletons. The later two methods aim at a whole body registration by non-rigid registration method without skeleton structure labeling.

*Di.Xiao@csiro.au; phone 61 2 97179893; http://www.aehrc.com/biomedical_imaging/

In this paper, we aim at addressing the whole body skeleton registration by point matching based surface registration. Point matching based surface registration, using 3D shape context has recently emerged as an alternative to intensity bases non-linear registration [6]. Given a set of points on a source surface, 3D shape context can provide the corresponding point locations on a target surface. Once the matching is established, warping of one surface to the other can be performed with a smooth deformation model.

Shape context was originally proposed by Belongie *et al.* for 2D graph matching [7], as it provided an effective way to compute the similarity between two point clouds. A first 3D shape context was built in [8] for measuring 3D shape similarity. Urschler *et al.* [5, 9, 10] extended 2D shape context to 3D and applied it in image registration area for lung surfaces and thoracic registration from CT images. Di *et al.* [11] added surface curvature information from shapes to improve the performance of 3D shape context based surface registration. Point mismatching has been reported as an issue in 2D object recognition [12, 13] and for 3D point matching [9]. In 3D shape context based registration application, a common method is to remove a percentage of highest cost correspondences [5, 9].

Because the joint structure of mouse skeleton and individual differences of mouse posture during CT scans, point mismatching is also present when applying 3D shape context model for finding point correspondences between mouse skeletons. Long distance point mismatching can cause severe surface distortion after registration and neighboring point mismatching within a small region can cause surface local stretching and folding. Therefore, a robust point matching by 3D shape context model is important for a correct mouse skeleton registration which is described in a separate publication at this conference. In this paper, we propose a framework of 3D shape context based non-rigid registration method for mouse whole body skeleton registration. A skeleton extracting and processing method is proposed for identifying a clean skeletons or templates for registration. An improved 3D shape context model is applied as a kernel of the non-rigid registration. A specific iterative registration procedure is developed for mouse whole body skeleton registration.

2. METHOD

In this paper, all mouse CT images were acquired by a same micro-CT/PET scanner. The mouse CT images were scanned for early stage tumor location and growth estimation. With a pre-defined scan protocol, the mice were positioned with a similar prone posture and their fore limbs were stretched forward along two sides of their heads. Their hind limbs were stretched backward with toes facing up.

2.1 Skeleton extraction and pre-processing

A pre-processing framework is proposed for processing mouse CT images and obtaining clean and usable mouse skeletons. Firstly, the raw mouse CT image noise is reduced by curvature flow denoising method, which uses level set algorithm [14], for preserving sharp boundaries and smoothing homogeneous regions. Then, the image is thresholded into a binary image with a fixed threshold (threshold value = 1950), obtained after experimentation and related to the Hounsfield units of the bone. Finally, a mesh set of mouse raw skeletons is generated by applying marching cubes surface construction algorithm [15] and triangulation method on the binary image.

A respiratory sensor is an accessory that is often needed for monitoring respiration of a mouse during CT/PET scan. Because of the similar image intensity values of the respiratory sensor and bones, the extracted meshes by abovementioned binary thresholding method can contain the sensor (as shown in Fig. 1(a)). By applying mesh searching and sorting on all meshes, the second largest mesh representing respiratory sensor can be identified and removed (Fig. 1(b)). After further removing some small trivial meshes, a clean mouse whole body skeleton can be obtained as shown in Fig. 1(c).

By applying the same mesh cleaning method, the largest mesh, which contains skull, spine and hind limbs, can be labelled. This largest mesh, which is named as "major skeleton" (Fig. 1(d)), is used in an initial step of mouse whole-body skeleton registration. By applying mesh shrinking method on the clean whole-body skeleton and projecting all points on the processed skeleton to the skeleton's longitudinal axis (direction from its inferior to superior), a 2D histogram (distribution of the points on the longitudinal axis) can be generated (Fig. 2). The minimal value on the histogram at lumbar vertebrae can be automatically detected and used as a feature point to cut the whole-body skeleton into two parts: hind-body skeleton (Fig. 1(e)) and fore-body skeleton (Fig. 1(f)). The hind-body skeleton is one single connected mesh. The fore-body skeleton consists of four independent meshes: vertebrae and head, left fore limb, right fore limb and sternum.

(a) A raw skeleton extracted from a binary image.

(b) A skeleton after respiratory sensor removal.

(c) A clean mouse whole body skeleton.

(d) A major skeleton after largest mesh selection.

(e) A fore-body skeleton.
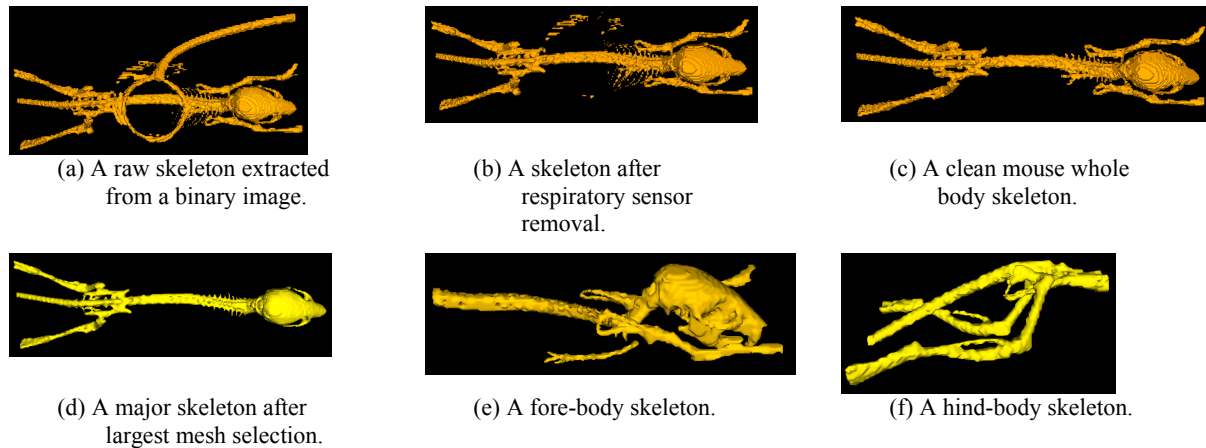
(f) A hind-body skeleton.

Fig. 1. Skeleton pre-processing and each part used in skeleton template.

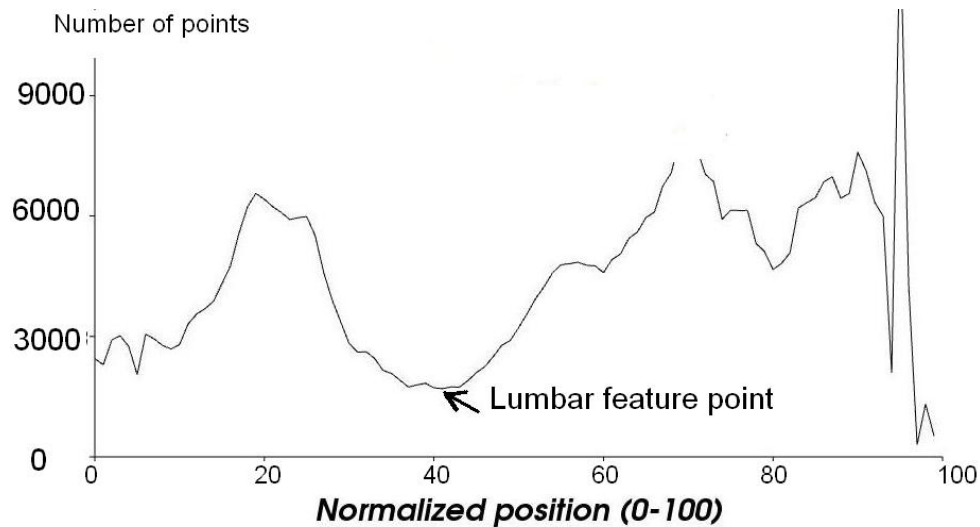

Fig. 2. 2D histogram of skeleton mesh point projection on skeleton longitudinal axis (from inferior 0 to superior 100) and lumbar feature point.

2.2 Preparation of skeleton Template

By using the pre-processing method, a scanned mouse CT image can be processed to generate a skeleton template or an atlas, which includes the following parts:

- a clean whole body skeleton (multiple meshes) without respiratory sensor and trivial meshes,

- a major skeleton (one mesh) which includes connective skull, vertebrae, hips and hind limb skeletons,

- a hind body skeleton which including hind part of vertebrae, hips and hind limb skeletons ,

- a fore body skeleton which including head, fore part of vertebrae, sternum and fore limb skeletons,

- a lumbar feature point which separates the hind body and fore body skeletons from their whole body skeleton.

Figs. 1(c) to 1(f) show each part of a complete mouse skeleton template. The template obtained by the method is used as a source skeleton to register to other mouse skeletons (target skeletons) in the experiments of the paper.

2.3 3D shape context based non-rigid registration

If M_S represents source surface and M_T represents target surface, the goal of a registration is to find a transform $\mathbf{t}: M_S \rightarrow M_T$. A triangular mesh representation $M(V, F)$ is used here, where V is the set of vertices (points in a mesh) and F the set of triangular faces of the mesh. Surfaces are usually high resolution meshes; therefore, landmarks (as low resolution vertices selected from the surfaces) are used to represent the surfaces. The transform is computed from the landmarks correspondences. In this paper, the landmarks are vertices from decimated triangular meshes, which are obtained from their high resolution triangular meshes by mesh decimation approach. A landmark mesh L has the relationship with its high resolution mesh M as $\{V \in L\} \subset \{V \in M\}$ and $\{F \in L\} \subset \{F \in M\}$. The decimation method ensures that the landmark vertices are uniformly distributed on the original high resolution meshes.

We apply an improved 3D shape context based non-rigid registration method in the framework of mouse whole body skeleton registration. The method was based on 3D shape context model but provided effective point mismatching correction algorithm, which uses topological structure correction (TSC) method for correcting long geodesic distance mismatch (LGDM) points and correspondence field smoothing (CFS) method for correcting neighbors crossing mismatch (NCM) points. Please see corresponding paper presented at this conference for details [16]. Here, the improved 3D shape context method is used for correct corresponding points matching between the source and target landmark meshes L_S and L_T by their landmark vertices V_S and V_T. A final source landmarks $V_S^f \in L_S$ and target landmarks V_T^f are obtained, and the correspondences between them are constructed.

After obtaining the correspondences between the two sets of landmark vertices V_S^f and V_T^f, the mapping of the source surface is modeled with a thin-plate spline (TPS) [17] for high resolution vertices mapping and constrained by the source surface's topology. The TPS model, describing the transformed point (x', y', z') independently as a function of original point (x, y, z) has the form:

$$(x', y', z') = t(x, y, z) = a_1 + a_2 x + a_3 y + a_4 z + \sum_{i=1}^{n} w_i U\left(\left|V_S^f(i) - (x, y, z)\right|\right) \tag{1}$$

where $U(r) = r^2 \log r$ is the basis function, $\mathbf{a} = \{a_1, a_2, a_3, a_4\}$ the global affine parameters of the transformation and $\mathbf{w} = \{w_1, ..., w_n\}$ the additional non-linear deformation. $V_S^f(i)$ ($i = 1, ..., N$) are source landmark vertices. N is the number of the source landmark vertices. Landmark vertices $V_S^f(i)$ and $V_T^f(i)$ are used to compute the coefficients $\mathbf{a}$ and $\mathbf{w}$ in the function by minimizing its bending energy [14]. With computed coefficients and source landmark vertices, a non-linear mapping function is built between the source and target vertex sets. Combined with the topology of the source mesh M_S, a transform $\mathbf{t}: M_S \rightarrow M_T$ is constructed.

2.4 An iterative procedure of non-rigid registration

Considering the relative large posture difference in mouse CT scan, a 4-step iterative procedure has been developed for mouse skeletons registration during implementing the improved 3D shape context non-rigid registration method.

The iterative procedure is illustrated in the diagram in Fig. 3. The initial source landmark mesh L_S and the target landmark mesh L_T are generated by mesh decimation algorithm from their respective high resolution meshes M_S and M_T. At the first iteration, the deformed landmark meshes are initialized from the original decimated meshes. During the steps 2 to 4, various matching correction techniques and applied successively. During all the steps the number of vertices and the topology are preserved

In the procedure, the correspondence field 1 is generated from the basic 3D shape context algorithm with one-to-one landmark vertex match between the deformed landmark set 1 and matched target landmark set 1. As described in section 2.3, the TSC algorithm uses mesh topology from source landmark mesh. In order to avoid re-computing the topology, the

topology of all vertices is preserved based on the source landmark mesh. A straightforward solution is to let the number of vertices on the source landmark mesh to be less than that of vertices on the target landmark mesh after their respective decimation processes. This avoids removing any vertices in the source landmark mesh during the process of 3D shape context computation. The correspondence field 1 preserves 100% of the cost, and the input of the TSC algorithm is the deformed landmark mesh with correspondence field 1.
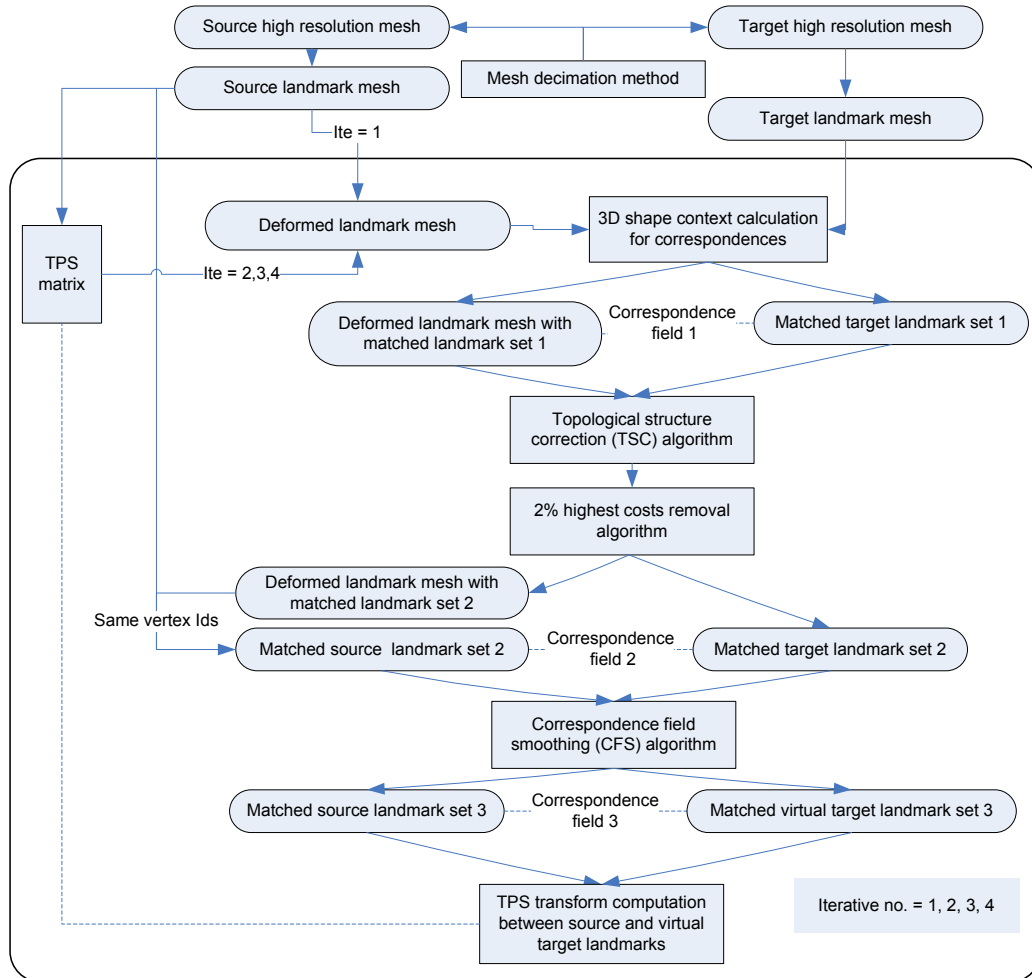

Fig. 3. An iterative procedure of the improved 3D shape context non-rigid registration.

After the TSC, long geodesic distance mismatch correspondences are removed from two landmark sets. In addition the 2% highest cost correspondences are removed as they correspond to obvious mismatching errors from our experiments. The result is a robust correspondence set between the two meshes. The deformed landmark mesh has the same topology (same vertices with their Ids in the mesh) as the source landmark mesh, a matched source landmark set 2 can be identified from the source landmark mesh by using the matched vertex Ids from the deformed landmark set 2. A correspondence field (correspondence field 2) between the matched source landmark set 2 and the matched target landmark set 2 is constructed. A CFS method is applied for smoothing the correspondence field 2 and generating correspondence field 3.

The smoothing filter kernels are set to 5, 4, 2 and 1 for the different iterations. The first iteration with large kernel size estimates a very smooth correspondence field that is subsequently relaxed to allow more precise matching of individual points. The very small kernel size of the last step ensures mostly that the deformation field does not contain any folding. In our experience, we found that the whole procedure had a stable convergence with excellent matching results. The TPS transform computed after the iterative procedure can be directly applied for the transformation of the source high

resolution mesh M_S, thereby interpolating the transformation to the whole image domain from the set of matching points.

2.5 A framework of mouse whole-body skeleton registration

To limit computation time and keep the memory requirement compatible with standard desktop computer memory we used 800 landmarks for the improved 3D shape context based non-rigid registration method. The registration uses a coarse-to-fine approach with the following steps:

(1).Skeleton extraction and pre-processing method on a mouse CT to obtain a clean mouse whole body skeleton.

(2) Initial registration of major skeletons from a template to that of the study by using the 3D shape context based non-rigid registration. Use the registration transform to map the lumbar feature points from the template to the clean skeleton and clipping a hind-body skeleton from the clean skeleton.

(3) Iterative fine-tuning registration from the hind-body skeleton template to the study's hind-body skeleton.

(4) Apply the registration transform from step (3) to map the lumbar point from the template to the clean skeleton and clipping a fore-body skeleton from the study. The remapping of the lumbar point provides an accurate fore-body clipping at the cutting point.

(5) Iterative fine registration from the fore-body skeleton template to the study's hind-body skeleton, using decreasing kernel sizes.

(6) Generation of the final TPS transform from the correspondence fields obtained from steps (3) and (5), and mapping of the whole-body skeleton from the template to the study.

3. EXPERIMENTS AND DISCUSSIONS

The proposed method was implemented using C++ language. In the experiments, we used the method in [18] and a surface measurement tool [19] to calculate mean absolute difference (MAD) error (mean absolute distance of all sampled points) and face root mean square (RMS) error (root mean square error of all sampled triangle faces) between two surfaces. 3 mice were scanned by micro-CT scanner. Each mouse was imaged with CT scan once every 4 or 5 days. 12 CT images (each mouse with 4 time points) were chosen for testing our method. For each CT image, the original image size was 384, 384, and 461 with an isotropic pixel resolution of 0.217 mm.

3.1 Mouse hind limb skeleton registration and intra- and inter-group comparison

The proposed method was applied for mouse hind limb skeleton registration. The skeleton from each mouse's first CT scan was used as the source skeleton. The registration experiments were grouped into 1) intra-subject registration: the first scan from each mouse was registered to its other three scans; and 2) inter-subject registration: each mouse's first scan was registered to a different mouse's three scans. For each registration process, α =0.6, β =0.55 and high cost preservation 98%. We used 800 landmarks, 4 iterations of registration process with respective median filter kernel 4, 4, 2 and 1.

Fig. 4 gives two examples of registered results from the intra-subject and inter-subject groups (Figs. 4(a) and 4(b)). Even with large posture difference as shown in Fig. 4(a), the method can obtain very good registration results. Fig. 5 shows the means and standard deviations of MAD and face RMS errors from the intra-subject group and inter-subject group. The mean MAD error from the intra-subject group is 0.16 mm with maximum 0.20 mm and minimum 0.13 mm, and the mean face RMS 0.20 mm with maximum 0.27 mm and minimum 0.16 mm. The mean MAD error from the inter-subject group is 0.17 mm with maximum 0.26 mm and minimum 0.13 mm, and the mean face RMS 0.23 mm with maximum 0.37 mm and minimum 0.17 mm. The large errors usually happened in the joint parts, as patella and calcaneus. Statistical results of *t*-Test based on MAD errors and face RMS errors did not find significant differences for the mean of errors from the inter-subject group compared to the intra-subject group.

(a) One registration result from intra-subject group (side view and top view).

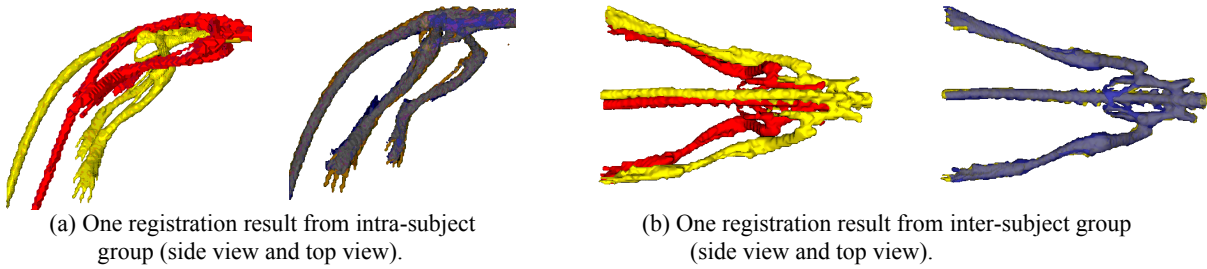(b) One registration result from inter-subject group (side view and top view).

Fig. 4. Results of mouse hind limb skeletons registration (red-source skeleton; yellow-target skeleton; blue-registered skeleton). (Please refer to color picture of the paper on CD-ROM from proceedings volumes).
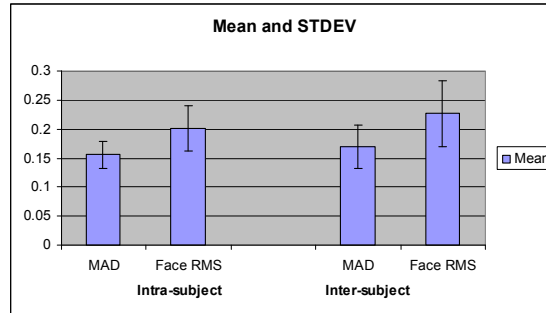

Fig. 5. Mean and standard deviation of registration errors from inter-subject and inter-subject groups

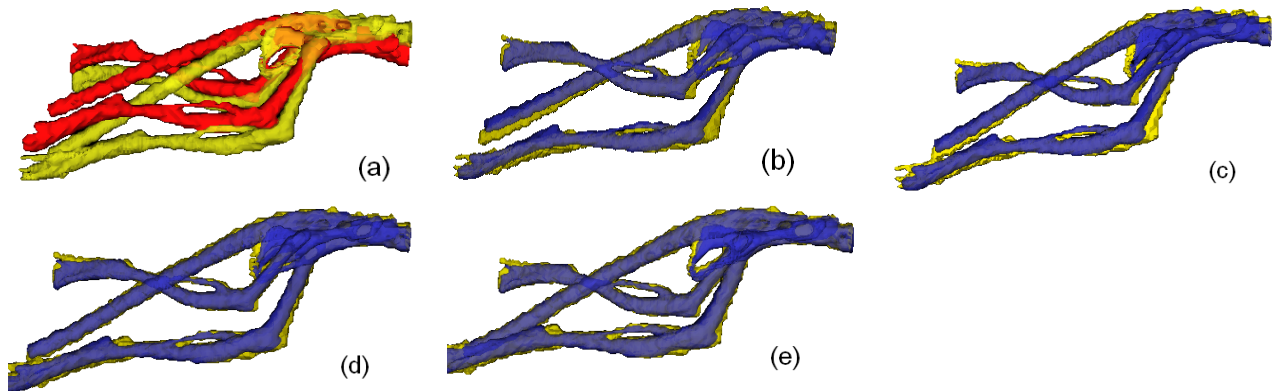## 3.2 Performance of iterative registration procedure

Fig. 6. Source surface approaching the target surface in an iterative procedure ((a) before iteration; (b) registered surface after iteration 1; (c) registered surface after iteration 2; (d) registered surface after iteration 3; (e) registered surface after iteration 4. red – source, yellow – target, and blue – registered surface). (Please refer to the color picture in the paper on CD-ROM from proceedings volumes).
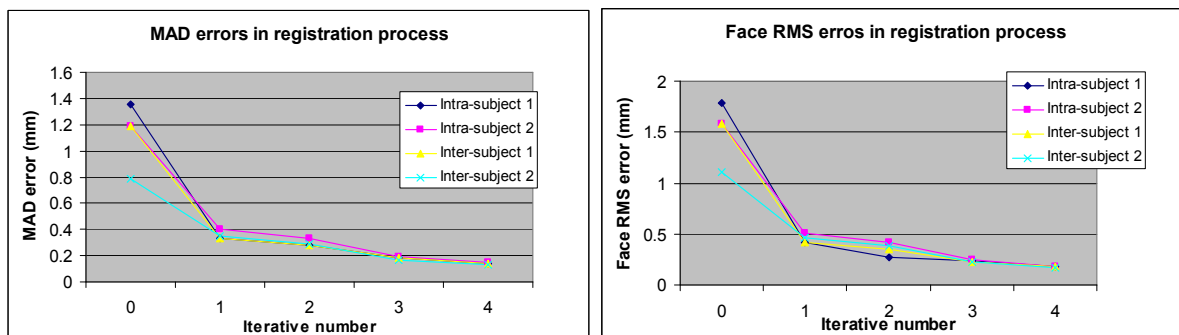

Fig. 7. Iterative registration process from inter-subject and inter-subject groups

An experiment was designed to test the convergence of the proposed iterative registration procedure. 4 iterations were adopted in the experiment with Gaussian kernel 5, 4, 2 and 1 respectively. Two pairs of samples each from the same mouse were used as intra-subject group and the other two pairs of samples from different mice as inter-subject group. Fig. 6 shows one example of registered surfaces (blue color) in each step of the iterative procedure. Fig. 7 shows the MAD and face RMS errors of the registered surfaces during the iterative process. It shows, after one iteration, there is an obvious error decrease then followed by a stable error decrease process in the rest of 3 iterations.

3.3 Mouse whole body skeleton registration

The proposed method was applied for mouse whole body skeleton registration. From the 12 CT images from 3 mice, We selected 8 pairs of CT images (each pair from same mouse) as intra-subject (IAS) group and 13 pairs of CT images (each pair from different mice) as inter-subject (IRS) group. The iterative number for all three processes was 4 with Gaussian kernel 5, 4, 2 and 1. Fig. 8 and Fig. 9 show two examples of registration results. Table 1 and Table 2 give the MAD and face RMS errors for total 21 pairs of registered skeletons. The registration results demonstrate that the proposed registration framework provides a robust and accurate registration for mouse skeletons.

Table 1 MAD and face RMS errors of mouse whole body skeleton registration in intra-subject group.

	Errors (mm)	IAS1	IAS2	IAS3	IAS4	IAS5	IAS6	IAS7	IAS8
Hind body skeleton	MAD	0.14	0.18	0.16	0.17	0.19	0.18	0.20	0.15
	Face RMS	0.18	0.25	0.20	0.23	0.19	0.22	0.26	0.20
Fore body skeleton	MAD	0.20	0.15	0.221	0.22	0.43	0.20	0.42	0.39
	Face RMS	0.29	0.20	0.30	0.29	0.18	0.25	1.14	1.06

Table 2 MAD and face RMS errors of mouse whole body skeleton registration in inter-subject group.

	Errors (mm)	IRS1	IRS2	IRS3	IRS4	IRS5	IRS6	IRS7	IRS8	IRS9	IRS 10	IRS 11	IRS 12	IRS 13
Hind body skeleton	MAD	0.17	0.18	0.19	0.19	0.19	0.20	0.27	0.19	0.16	0.15	0.22	0.14	0.15
	Face RMS	0.22	0.24	0.24	0.26	0.26	0.15	0.36	0.25	0.22	0.19	0.30	0.18	0.19
Fore body skeleton	MAD	0.35	0.23	0.38	0.22	0.53	0.25	0.16	0.19	0.65	0.20	0.41	0.17	0.21
	Face RMS	0.26	0.31	0.63	0.28	1.43	0.33	0.21	0.25	0.42	0.30	0.62	0.25	0.28

Fig. 8. A mouse whole body skeleton registration result from inter-subject group (red – source; yellow – target; blue – registered skeleton). (Please refer to the color picture in the paper on CD-ROM from proceedings volumes).

Fig. 9. A mouse whole body skeleton registration result from intra-subject group (red – source; yellow – target; blue – registered skeleton). (Please refer to the color picture in the paper on CD-ROM from proceedings volumes).

4. CONCLUSIONS

We proposed an automatic mouse whole body skeleton registration method based on our improved 3D shape context non-rigid registration. The registration framework for mouse whole body skeleton registration demonstrated the coarse-to-fine step and iterative procedure in each registration step achieved a stable registration process and an accurate

registration result. The registration method was robust for both inter-subject registration and intra-subject registration. The registration method can be applied for other organs registration of small animals, as lung and skin and the registration results can be used as an initial step for small animal whole body organs registration or volume image registration.

REFERENCES

1. M. Baiker, J. Milles, A.M. Vossepoel, I. Que, E.L. Kaijzel, C.W.G.M. Lowik, J.H.C. Reiber, J. Dijkstra and B.P.F. Lelieveldt, "Fully Automated whole-body registration in mice using an articulated skeleton atlas," ISBI, 728-731 (2007).
2. X. Li, T.E. Peterson, J.C. Gore, B.M. Dawant, "Automatic registration of whole body serial micro CT images with a combination of point-based and intensity-based registration techniques," ISBI 2006, 454-457 (2006).
3. H. Chui and A. Rangarajan, "A new point matching algorithm for non-rigid registration," Computer vision and Image Understanding, 114-141 (2003).
4. S. Gold, A. Rangarajan, C.P. Lu, S. Pappu, E. Mjolsness, "New algorithms for 2D and 3D point matching: pose estimation and correspondence," Pattern Recognition 31(8), 1019-1031 (1998).
5. H. Wang and B. Fei, "A robust B-Splines-based point match method for non-rigid surface registration," Proc. of the 2nd International Conference on Bioinformatics and Biomedical Engineering, 2353-2356 (2008).
6. M. Urschler, H. Bischof, "Registering 3D lung surfaces using the shape context approach," Proc. Medical Image Understanding and Analysis, 212-215 (2004).
7. S. Belongie, J. Malik and J. Puzicha, "Matching Shapes," Proc. Eighth Int'l. Conf. Computer Vision, 454-461 (2001).
8. M. Kortgen, G. Park, M. Novotni, R. Klein, "3D Shape Matching with 3D Shape Context," Seventh Central European Seminar on Computer Graphics (2003).
9. M. Urschler, J. Bauer, H. Ditt, H. Bischof, "SIFT and Shape Context for Feature-Based Nonlinear Registration of Thoracic CT Images," Proc. Computer Vision Approaches to Medical Image Analysis, 73-84 (2006).
10. M. Urschler, H. Bischof, "Assessing breathing motion by shape matching of lung and diaphragm surfaces," Proceedings of the SPIE Medical Imaging, 5746, 440-452 (2005).
11. D. Xiao, P.T. Bourgeat, J.E. Fripp, O.A. Tamayo, M. Gregoire, O. Salvado, "Non-rigid registration of small animal skeletons from micro-CT using 3D shape context," Proc. of SPIE Medical Imaging, 7259, 72591G (2009).
12. A. Thayananthan, B. Stenger, P.H.S. Torr, and R. Cipolla, "Shape Context and Chamfer Matching in Cluttered Scenes," Proc. IEEE Conf. Computer Vision and Pattern Recognition, 1, 127-133 (2003).
13. S. Giannarou, and T. Stathaki, "Object Identification in Complex Scenes using Shape Context Descriptor and Multi-stage Clustering," 15th International Conference on Digital Signal Processing, 244-247 (2007).
14. J.A. Sethian, Level set methods and fast marching methods, Cambridge Press, chapter 16, Second edition (1999).
15. W. Lorensen and H. Cline, "Marching cubes: a high resolution 3D surface construction algorithm," Computer Graphics, 21, 163-169 (1987).
16. D. Xiao, D. Zahra, P. Bourgeat, P. Berghofer, O. Acosta Tamayo, C. Wimberley, M. Gregoire, O. Salvado, "An improved 3D shape context registration method for non-rigid surface registration," Proc. of SPIE Medical Imaging, (2010) (Accepted).
17. F.L. Bookstein, "Principal warps: Thin-plate splines and the decomposition of deformation," IEEE Trans. PAMI, 11(6), 567-585 (1989).
18. N. Aspert, D. Santa-Cruz, T. Ebrahimi, "MESH: Measuring Errors between Surfaces using the Hausdorff distance," the proceedings of the IEEE Int. Conf. on Multimedia and Expo (ICME), I, 705-708 (2002).
19. http://www.cs.unc.edu/~xushun/research/MeshValmet.html.